Inorg. Chem. **2005**, *44*, 8234–8242

Structural and Spectroscopic Features of Mono- and Binuclear Nickel(II) Complexes with Tetradentate $N(amine)_2S(thiolate)_2$ Ligation

Robert T. Stibrany, Stephen Fox,[†] Parimal K. Bharadwaj,[‡] Harvey J. Schugar,* and Joseph A. Potenza*

Department of Chemistry and Chemical Biology, Rutgers, The State University of New Jersey, 610 Taylor Road, Piscataway, New Jersey 08854

Received January 24, 2005

Three complexes containing $Ni^{II}N(amine)_2S(thiolate)_2$ units have been prepared and characterized. Both (*R*,*R*)-*N*,*N*′-bis(1-carboxy-2-mercaptoethyl)-1,2-diaminoethane [(*R*,*R*)-**1**] and *N*,*N*′-bis(2-methyl-2-mercaptoprop-1-yl)-1,3-diamino-2,2-dimethylpropane (**4**) act as tetradentate S–N–N–S ligands to form complexes Ni((*R*,*R*)-**1**) and Ni(**4**) with nearly planar *cis*-NiN_2S_2 units. The N–Ni–N and S–Ni–S angles differ significantly in the two complexes yet are very nearly supplementary. The 1,3-disubstituted cyclohexane species *rac*-*N*,*N*′-bis(2-mercapto-2-methylprop-1-yl)-1,3-cyclohexanediamine (**6**) behaves as a bis(bidentate-*N*,*S*) ligand to form an unexpectedly intense-blue dinickel complex (1*S**,3*R**,1′*S**,3′*R**)-**7**, which contains two *trans*-NiN_2S_2 units bridged by 1,3-disubstituted cyclohexane groups. The coordination geometry in (1*S**,3*R**,1′*S**,3′*R**)-**7** is distorted 15° toward tetrahedral, most likely as a result of steric crowding, suggested by several short contacts between the NiS_2 units and both the cyclohexyl and *gem*-dimethyl groups of the N,S-chelate rings. The complexes exhibit rich UV–vis spectra, whose deconvoluted bands are now fully assigned, from low to high energy, as ligand field (LF), π(S) → Ni(II) ligand-to-metal charge transfer (LMCT), σ(S) → Ni(II) LMCT, σ(N) → Ni(II) LMCT, localized S, and S,N Rydberg transitions. The unusually intense LF absorptions shown by (1*S**,3*R**,1′*S**,3′*R**)-**7** are thought to result from relaxation of the Laporte restriction arising from the 15° tetrahedral twist.

Introduction

The bioinorganic chemistry of nickel metalloenzymes continues to attract considerable interest. Recent advances include structural characterizations of the *cis*-$NiN_2S(thiolate)_2$ subunits in the active sites of an acetyl−coenzyme A synthase/CO dehydrogenase[1,2] and a nickel superoxide dismutase.[3] These studies have prompted renewed interest in NiN_2S_2 complexes that mimic the properties of native nickel metalloproteins.[4−12] The so-called A cluster, which is the active site of acetyl coenzyme A, has been of particular interest. This novel site contains a *cis*-$NiN_2S(thiolate)_2$ unit linked to a cuboidal Fe_4-S_4 cluster by a bridging metal ion, which can be iron, nickel, or zinc.

* To whom correspondence should be addressed. E-mail: schugar@rutchem.rutgers.edu (H.J.S.), potenza@rutchem.rutgers.edu (J.A.P.).

[†] Current address: Department of Chemistry, University of Louisiana at Monroe, Monroe, LA 71209.

[‡] Current address: Indian Institute of Technology, Kanpur 208016, India.

(1) Doukov, T. I.; Iverson, T. M.; Seravalli, J.; Ragsdale, S. W.; Drennan, C. L. *Science* **2002**, *298*, 567−572.

(2) Darnault, C.; Volbeda, A.; Kim, E. J.; Legrand, P.; Vernède, X.; Lindahl, P. A.; Fontecilla-Camps, J. C. *Nat. Struct. Biol.* **2003**, *10*, 271−279.

(3) (a) Barondeau, D. P.; Kassmann, C. J.; Bruns, C. K.; Tainer, J. A.; Getzoff, E. D. *Biochemistry* **2004**, *43*, 8038−8047. (b) Wuerges, J.; Lee, J.-W.; Yim, Y.-I.; Yim, H.-S.; Kang, S.-O.; Carugo, K. D. *Proc. Natl. Acad. Sci. U.S.A.* **2004**, *101*, 8569−8574.

(4) Krishnan, R.; Riordan, C. G. *J. Am. Chem. Soc.* **2004**, *126*, 4484−4485.

(5) Hatlevik, O.; Blanksma, M. C.; Mathrubootham, V.; Arif, A. M.; Hegg, E. L. *J. Biol. Inorg. Chem.* **2004**, *9*, 238−246.

(6) Harrop, T. C.; Olmstead, M. M.; Mascharak, P. K. *Chem. Commun.* **2004**, 1744−1745.

(7) Golden, M. L.; Rampersad, M. V.; Reibenspies, J. H.; Darensbourg, M. Y. *Chem. Commun.* **2003**, 1824−1825.

(8) Wang, Q.; Blake, A. J.; Davies, E. S.; McInnes, E. J. L.; Wilson, C.; Schröder, M. *Chem. Commun.* **2003**, 3012−3013.

(9) (a) Szilagyi, R. K.; Bryngelson, P. A.; Maroney, M. J.; Hedman, B.; Hodgson, K. O.; Solomon, E. I. *J. Am. Chem. Soc.* **2004**, *126*, 3018−3019. (b) Maroney, M. J.; Choudhury, S. B.; Bryngelson, P. A.; Mizra, S. A.; Sherrod, M. J. *Inorg. Chem.* **1996**, *35*, 1073−1076.

(10) Rao, P. V.; Bhaduri, S.; Jiang, J.; Holm, R. H. *Inorg. Chem.* **2004**, *43*, 5833−5849.

(11) (a) Webster, C. E.; Darensbourg, M. Y.; Lindahl, P. A.; Hall, M. B. *J. Am. Chem. Soc.* **2004**, *126*, 3410−3411. (b) Bellefeuille, J. A.; Grapperhaus, C. A.; Derecsk ei-Kovacs, A.; Reibenspies, J. H.; Darensbourg, M. Y. *Inorg. Chim. Acta* **2000**, *300*, 73−81.

(12) Grapperhaus, C. A.; Mullins, C. S.; Kozlowski, P. M.; Mashuta, M. S. *Inorg. Chem.* **2004**, *43*, 2859−2866.

10.1021/ic050114h CCC: $30.25
Published on Web 10/15/2005

Owing to the ease of forming thiolate-bridged metal complexes, a growing array of polynuclear complexes have been reported, which contain *cis*-$NiN_2S(thiolate)_2$ subunits linked by nickel, zinc, iron, or copper ions.[10] The chemistry of *cis*-$NiN_2S(thiolate)_2$ units also has applications beyond that of nickel biochemistry. In addition to studying Cu(I)-[13] and Ni(I)-bridged[14] adducts of such units, we have used them to synthesize macrocyclic bis(disulfide) chelating agents[15] and, in one instance, as a diamagnetic host for studies of a remarkably stable *cis*-$Cu^{II}N_2S(thiolate)_2$ complex.[16] We present here the structural and spectroscopic characterizations of three $NiN_2S(thiolate)_2$ complexes, which have been used in the above endeavors. One of these complexes exhibits a surprisingly intense-blue color, whose origin we sought to determine.

Experimental Section

General Procedures and Methods. Reagents were used as received from commercial suppliers or were purified by standard methods.[17] Reactions were carried out under atmospheric conditions unless otherwise noted. Melting points were determined with a hot-stage apparatus and are uncorrected. Infrared spectra were measured using a Mattson Galaxy series 5000 spectrophotometer. Conventional and circular dichroism (CD) electronic spectral measurements were made using Cary instruments that were upgraded and computer-interfaced by Aviv Associates. Low-temperature electronic (80 K) spectra were measured using an Air Products optical Dewar. Magnetic susceptibility measurements were made over the 10−300 K range using a Quantum Design SQUID magnetometer operated at an applied field of 1000 G. Diamagnetic corrections were applied to the susceptibilities. ^{13}C and ^{1}H NMR spectra were recorded at room temperature using Varian XL-400 and Bruker AVANCE 400 Ultrashield spectrometers.

1. Preparation of the Complexes. The preparations of Ni((*R*,*R*)-**1**), Ni(**4**), and (1*S**,3*R**,1′*S**,3′*R**)-**7**·2DMF are outlined in Scheme 1.

(*R*,*R*)-*N*,*N*′-Bis(1-carboxy-2-mercaptoethyl)-1,2-diaminoethanenickel(II) *N*,*N*′-1,3-Diammoniumpropane Trihydrate, [$H_3N(CH_2)_3NH_3$][Ni((*R*,*R*)-1]·3H_2O. Addition of 1,3-diaminopropane (0.16 g, 1 mmol) to a slurry of $NiCl_2·6H_2O$ (0.23 g, 0.96 mmol) and *N*,*N*′-ethylenebis(L-cysteine) [H_4(*R*,*R*)-**1**;[18] 0.27 g, 1.0 mmol] in 3 mL of H_2O afforded a slightly basic (pH ∼ 8) brown solution. Following the addition of 5 g of dimethylformamide (DMF), the mixture was quickly filtered (medium frit) and evaporated in air to yield orange crystalline rectangular blades (yield: 0.30 g, 66%), which exhibited yellow−orange dichroism when polarized light was directed perpendicular and parallel, respectively, to the long dimension. The density [1.53(1) g/cm^3] of the orange crystals was measured by flotation in a mixture of carbon tetrachloride and heptane.

1,8-Diaza-4,5-dithia-3,3,6,6,10,10-hexamethylcycloundeca-(1*E*,7*E*)-diene (3). A solution of 2,2-dimethyl-l,3-propanediamine (16.6 g, 0.163 mol) in 50 mL of heptane was added to bis(2-methyl-1-oxo-2-propyl) disulfide[15] (**2**; 33.6 g, 0.163 mol) in 100 mL of heptane. The system was degassed, refluxed for 2 h under argon, and stripped to dryness to yield 40 g of an orange paste, 10 g of which was sublimed twice to yield 0.2 g (0.4%) of the Schiff base **3** as a white crystalline solid (mp 93−94 °C).

Scheme 1. Syntheses of the Complexes

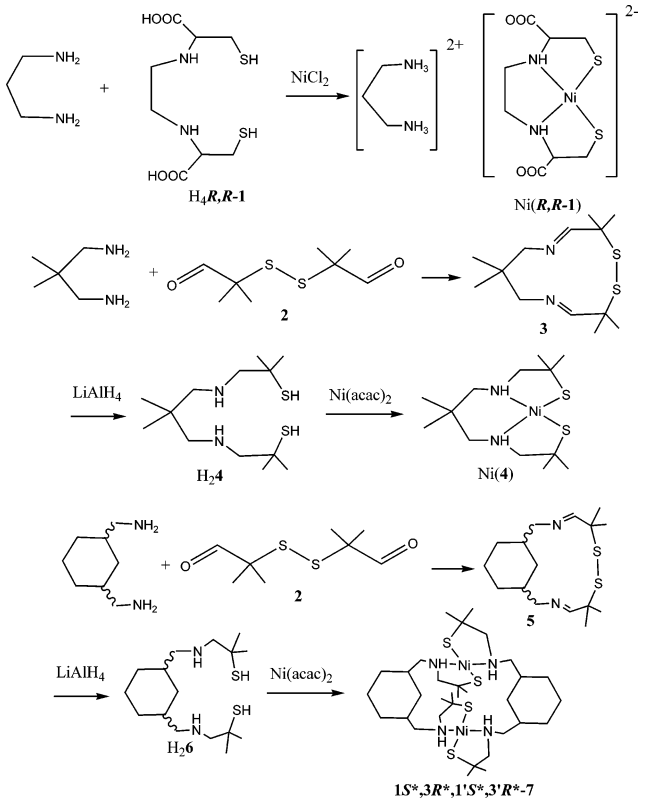

***N*,*N*′-Bis(2-methyl-2-mercaptoprop-1-yl)-1,3-diamino-2,2-dimethylpropane ($H_2$4).** A solution of crude **3** (14 g, 51 mmol) in 100 mL of tetrahydrofuran (THF) was added cautiously and with vigorous stirring to lithium aluminum hydride (3.93 g, 102 mmol) in 100 mL of THF. The mixture was refluxed for 12 h, cooled to −78 °C, quenched with 30 mL of a saturated sodium sulfate solution, and allowed to warm to room temperature with vigorous stirring (3 h). Diethyl ether (120 mL) was added to the sodium sulfate solution to reduce the viscosity. The resulting white gelatinous precipitate was filtered, and the filtrate was dried over powdered magnesium sulfate and stripped to yield H_2**4** (yield: 2.85 g, 20%) as a clear yellow oil. ^{1}H NMR ($CDCl_3$): δ 2.58 (s, 4H), 2.51 (s, 4H), 1.72 (br s, 4H), 1.35 (s, 12H), 0.94 (s, 6H). ^{13}C NMR ($CDCl_3$): δ 64.5, 60.0, 45.8, 35.6, 30.5, 24.7.

***N*,*N*′-Bis(2-methyl-2-mercaptoprop-1-yl)-1,3-diamino-2,2-dimethylpropanenickel(II) [Ni(4)].** Solutions of nickel acetyl acetonate [$Ni(acac)_2$; 0.750 g, 2.92 mmol] in 25 mL of methylene chloride and of H_2**4** (1.11 g, 4.0 mmol) in 25 mL of methylene chloride were combined and evaporated under vacuum to yield a brown paste. Addition of diethyl ether (25 mL) converted the brown paste to a brown powder, which was collected by filtration, washed with diethyl ether (25 mL), and dried in vacuo to yield crude, microcrystalline Ni(**4**) (yield: 0.98 g, 100%), 0.2 mmol of which was recrystallized from acetone/isooctane to yield red-brown crystals suitable for X-ray diffraction. The density [1.31(1) g/cm^3] was measured by flotation in a mixture of carbon tetrachloride and isooctane. IR (KBr pellet, cm^{-1}): 2955 s, 2911 s, 2857 s, 1625 w, 1446 m, 1384 m, 1357 m, 1125 m, 1045 m, 1009 m, 938 m.

(13) (a) Fox, S.; Stibrany, R. T.; Potenza, J. A.; Schugar, H. J. *Acta Crystallogr.* **1996**, *C52*, 2731−2734. (b) Stibrany, R. T.; Schugar, H. J.; Potenza, J. A. *Acta Crystallogr.* **2003**, *E59*, m630−m632.
(14) Fox, S.; Stibrany, R. T.; Potenza, J. A.; Schugar, H. J. *Inorg. Chim. Acta* **2001**, *316*, 122−126.
(15) Fox, S.; Stibrany, R. T.; Potenza, J. A.; Knapp, S.; Schugar, H. J. *Inorg. Chem.* **2000**, *39*, 4950−4961.
(16) Bharadwaj, P. K.; Potenza, J. A.; Schugar, H. J. *J. Am. Chem. Soc.* **1986**, *108*, 1351−1352.
(17) Perrin, D. D.; Armarego, W. L. F. *Purification of Laboratory Chemicals*; Pergamon Press: New York, 1988.
(18) Blondeau, P.; Berse, C.; Gravel, D. *Can. J. Chem.* **1967**, *45*, 49−52.

Table 1. Crystallographic Data for the Complexes Studied

	$[H_3N(CH_2)_3NH_3]Ni((R,R)\text{-}\mathbf{1})\cdot 3H_2O$	$Ni(\mathbf{4})_{233}$	$Ni(\mathbf{4})_{298}$	$(1S^*,3R^*,1'S^*,3'R^*)\text{-}\mathbf{7}\cdot 2DMF$
formula	$NiS_2O_7N_4C_{11}H_{24}$	$NiS_2N_2C_{13}H_{28}$	$NiS_2N_2C_{13}H_{28}$	$Ni_2S_4O_2N_6C_{38}H_{78}$
fw	455.24	335.22	335.22	896.72
a, Å	8.0080(8)	11.7710(15)	11.852(2)	10.435(7)
b, Å	13.371(3)	14.0419(17)	14.115(3)	10.702(1)
c, Å	18.151(4)	10.8293(13)	10.878(2)	12.251(3)
α, deg	90.	90.	90.	94.87(1)
β, deg	90.	111.946(4)	111.50(3)	111.17(1)
γ, deg	90.	90.	90.	107.785(7)
V, Å^3	1943.5(7)	1671.7(4)	1693.2(7)	1182.4(7)
space group	$P2_12_12_1$	$P2_1/c$	$P2_1/c$	$P\bar{1}$
Z	4	4	4	1
ρ_{calc}, g/cm^3	1.528	1.332	1.315	1.256
ρ_{obs}, g/cm^3	1.53(1)		1.31(1)	1.25(1)
μ, mm^{-1}	1.3	1.4	1.4	1.0
trans factor	0.95−1.00	0.83−1.00	0.76−1.00	0.89−1.00
T, K	298(1)	233(1)	298(1)	297(1)
data used in refinement	1976	2408	2344	2127
R_F,[a] R_{wF^2}[b]	0.039, 0.107	0.030, 0.076	0.031, 0.083	0.050, 0.139

[a] $R_F = \sum||F_o| - |F_c||/\sum|F_o|$; selection criterion $I > 2\sigma(I)$. [b] $R_{wF}^2 = \{[\sum[w(|F_o^2 - F_c^2|)/\sum[w(F_o^2)]\}^{1/2}$; selection criterion all F_o^2.

***rac*-1,8-Diaza-4,5-dithia-3,3,6,6-tetramethyl-9,11-butanocycloundeca-(1*E*,7*E*)-diene (5).** A solution of 1,3-diaminomethylcyclohexane (mixture of cis and trans isomers, 7.24 g, 51 mmol) in 100 mL of heptane was added dropwise to a solution of **2** (10.6 g, 51 mmol) in l00 mL of heptane. The mixture was refluxed for 2 h, cooled to ambient temperature under nitrogen, stripped of solvent by rotary evaporation, and dried in vacuo to give the oil **5** in quantitative yield as a mixture of isomers. ^{13}C NMR ($CDCl_3$): δ 166.4 (C═N), 51.7, 38.5, 29.5, 25.0, 24.9, 20.9, 18.4.

***rac*-*N*,*N*′-Bis(2-mercapto-2-methylprop-1-yl)-1,3-cyclohexanediamine ($H_2$6).** Oil **5** (15.9 g) was dissolved in 100 mL of freshly distilled THF, added to a suspension of lithium aluminum hydride (4 g, 105 mmol) in 100 mL of THF, refluxed overnight, cooled to −78 °C, and quenched as above with 30 mL of a saturated sodium sulfate solution. Following the addition of 100 mL of diethyl ether, the pH was lowered to about 8 by adding 150 mL of 1 M hydrochloric acid with stirring. The solution was filtered and washed with water to yield aqueous and organic layers, which were separated. The aqueous layer was extracted with additional diethyl ether, and the organic layers were combined, dried over magnesium sulfate, rotary evaporated, and dried in a vacuum to yield 11.3 g (35.7 mmol, 70.1%) of H_2**6** as an orange oil. ^{1}H NMR ($CDCl_3$): δ 3.73 (m, 2H), 2.57 (m, 10H), 1.85 (m, 8H), 1.36 (m, 14H). ^{13}C NMR ($CDCl_3$): δ 67.9, 63.6, 57.4, 45.6, 37.7, 31.5, 30.6, 25.5.

Bis[μ_2-(*N*,*N*′-bis(2-mercapto-κ^1Ni′,κ^1Ni″-2-methylprop-1-yl)-(1*Sκ^1Ni′,3*R**κ^1Ni″)-cyclohexanediamine)nickel(II)]·2DMF Solvate ((1*S**,3*R**,1′*S**,3′*R**)-7·2DMF).** (1*S**,3*R**,1′*S**,3′*R**)-**7**·2DMF was prepared from H_2**6** and $Ni(acac)_2$ in a manner analogous to the preparation of Ni(**4**) described above. A solution of $Ni(acac)_2$ (0.124 g, 0.48 mmol) in 10 mL of DMF was added under nitrogen to a solution of H_2**6** (0.212 g, 0.66 mmol) in 8 mL of DMF and was allowed to stand for 2 h, during which time crystals formed. Recrystallization of the crude product from hot (120 °C) DMF under nitrogen yielded well-formed blue prisms (yield: 0.073 g, 34%, based on Ni) suitable for X-ray diffraction. The density [1.25(1) g/cm^3] of the crystals was measured by flotation in a mixture of carbon tetrachloride and heptane. IR (KBr pellet, cm^{-1}): 3518 m, 3384 m, 3148 m, 2918 s, 2661 sh, 1635 m, 1447 s, 1362 m, 1169 m, 1056 s, 1042 s, 634 m.

2. Crystallography. For $[H_3N(CH_2)_3NH_3]Ni((R,R)\text{-}\mathbf{1})\cdot 3H_2O$, $Ni(\mathbf{4})_{298}$, and (1*S**,3*R**,1′*S**,3′*R**)-**7**·2DMF, diffraction measurements were made on an Enraf-Nonius CAD-4 diffractometer, and the Nonius Structure Determination Package[19] was used for data collection and processing. Graphite-monochromated Mo Kα radiation (λ = 0.710 73 Å) was used, and Lorentz, polarization, decay, and absorption corrections[20] were applied. For $Ni(\mathbf{4})_{233}$, diffraction measurements were made with a Bruker SMART CCD area detector system using φ and ω scans. A hemisphere of data was collected. Cell parameters were determined using the SMART software.[21] The SAINT package[22] was used for integration of data, for Lorentz, polarization, and decay corrections, and for merging of the data. Absorption corrections were applied using the program SADABS.[23]

All structures were solved and refined on F^2 using the SHELX system and all data.[24,25] Partial structures were obtained by direct methods, while the remaining non-H atoms were located using difference Fourier techniques. Except for the H atoms of the water molecules in Ni((*R*,*R*)-**1**), which were not located, all H atoms were located on difference maps or placed at calculated positions and were refined when possible. Views of the structures were prepared using ORTEP32 for Windows.[26,27] The crystals were mounted on glass rods, except for (1*S**,3*R**,1′*S**,3′*R**)-**7**·2DMF, which was mounted in a capillary tube containing DMF well removed from the crystal. All non-H atoms were refined anisotropically. Additional crystallographic details are given in Table 1 and as Supporting Information.

Results and Discussion

Description of the Structures. The structure of $[H_3N(CH_2)_3NH_3]Ni((R,R)\text{-}\mathbf{1})\cdot 3H_2O$ contains propanediammonium dications, Ni((*R*,*R*)-**1**) dianions (Figure 1), and three water molecules of solvation per asymmetric unit. These species are linked by an extensive intra- and interspecies, polymeric hydrogen-bonding network, which involves the four N atoms

(19) *Enraf-Nonius Structure Determination Package*; Enraf-Nonius: Delft, Holland, 1985.
(20) North, A. C. T.; Phillips, D. C.; Mathews, F. S. *Acta Crystallogr.* **1968**, *A24*, 351−359.
(21) *SMART-WNT2000*, version 5.622; Bruker AXS Inc.: Madison, WI, 2000.
(22) *Saint-Plus*, version 6.02; Bruker AXS Inc.: Madison, WI, 2000.
(23) Blessing, R. H. *Acta Crystallogr.* **1995**, *A51*, 33−38.
(24) Sheldrick, G. M. *SHELXS-97. Acta Crystallogr.* **1990**, *A46*, 467−473.
(25) Sheldrick, G. M. *SHELXL-97. A Computer Program for the Refinement of Crystal Structures*; University of Göttingen: Göttingen, Germany, 1997.
(26) Farrugia, L. J. *J. Appl. Crystallogr.* **1997**, *30*, 565.
(27) Burnett, M. N.; Johnson, C. K. *ORTEPIII*; Report ORNL-6895; Oak Ridge National Laboratory: Oak Ridge, TN, 1996.

Table 2. Metric Parameters for the Several Species Studied (Å, deg)

	$[H_3N(CH_2)_3NH_3]$Ni((*R*,*R*)-**1**)·3H$_2$O	Ni(**4**)$_{233}$	Ni(**4**)$_{298}$	(1*S**,3*R**,1′*S**,3′*R**)-**7**·2DMF
Ni−S1	2.1563(16)	2.1547(7)	2.1544(9)	2.201(2)
Ni−S2	2.1499(16)	2.1625(7)	2.1626(11)	2.2031(18)
Ni−N1	1.925(5)	1.974(2)	1.974(2)	1.945(6)
Ni−N2	1.936(5)	1.970(2)	1.970(2)	1.936(6)
S1−Ni−S2	94.03(6)	88.10(3)	88.29(4)	166.18(7)
S1−Ni−N1	89.29(16)	89.75(6)	89.81(7)	92.33(17)
S1− Ni−N2	174.65(17)	175.23(7)	175.25(8)	88.37(17)
S2−Ni−N1	174.05(16)	173.51(7)	173.36(8)	88.79(16)
S2−Ni−N2	89.16(15)	89.79(6)	89.63(7)	91.83(17)
N1− Ni−N2	87.9(2)	92.80(8)	92.73(10)	174.51(19)
Ni−S−C	99.76(19)	99.00(8)	99.11(9)	95.4(2)
	98.91(18)	98.26(8)	98.38(10)	95.4(2)
S1−Ni−S2/N1−Ni−N2	6.68(8)	7.32(9)	7.51(10)	15.00(18)[a]
S1···S2	3.150(2)	3.002(1)	3.007(2)	4.375(2)
ligand denture	S−N−N−S	S−N−N−S	S−N−N−S	S−N
chelate rings	5−5−5	5−6−5	5−6−5	5−16−5

[a] Dihedral angle S1−Ni−N2/S2−Ni−N1 (see Figure 3).

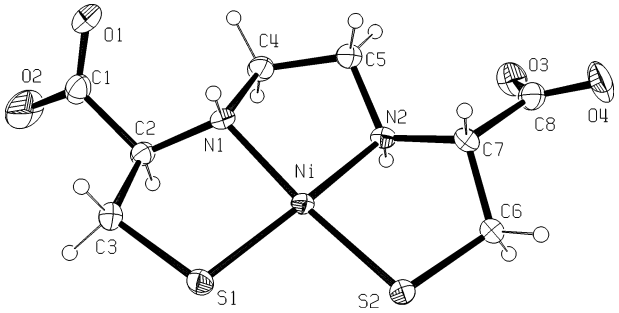

Figure 1. ORTEP[27] view of the dianion Ni((*R*,*R*)-**1**) shown with 30% probability thermal ellipsoids.

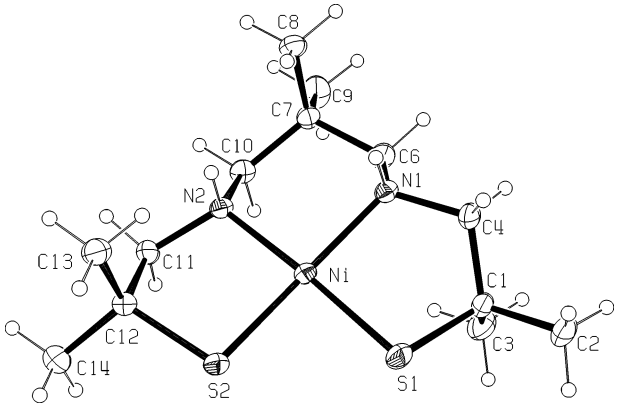

Figure 2. ORTEP[27] view of Ni(**4**)$_{233}$ shown with 30% probability thermal ellipsoids.

of the cation and anion, the two S atoms, the carboxylate O atoms, and the O atoms of the three water molecules. In contrast, the structure of Ni(**4**) (Figure 2) consists of discrete molecules linked by a single intermolecular N1−H(1N)···S2 hydrogen bond. Both Ni((*R*,*R*)-**1**) and Ni(**4**) exhibit distorted-square-planar *cis*-NiN(amine)$_2$S(thiolate)$_2$ coordination, with angular deviations from the ideal symmetry of less than 7° in all cases (Table 2). Further, the tetrahedral-twist dihedral angles (S1−Ni−S2/N1−Ni−N2) are both relatively small and within 1 degree of each other. In both species, the five-membered N,S-chelate rings adopt distorted envelope conformations, with the flaps, C2 and C7 for Ni((*R*,*R*)-**1**) and C1 and C12 for Ni(**4**), directed toward opposite sides of the NiN_2S_2 units.

Table 3. Metric Parameters (Å, deg) for Selected *cis*- and *trans*-Ni^{II}N$_2$S(thiolate)$_2$ Species

cis species	ref	N,N ring size	Ni−S	Ni−N	N−Ni−N	S−Ni−S
10, R = ethyl	31	6	2.1724(14)	2.0169(14)	98.00(1)	84.20(2)
			2.1757(6)	2.0201(15)		
10, R = methyl	32	6	2.176(1)	1.999(3)	97.3(1)	85.37(4)
			2.174(1)	2.006(3)		
13	35	0	2.155(3)	1.956(9)	91.6(4)	90.8(1)
			2.147(3)	1.949(9)		
8, R = CH_3	30	6,6	2.159(3)	1.995(3)	90.4	88.8
8, R = H	29	6,6	2.159(2)	1.985(6)	89.8(3)	89.5(1)
11, X = O═	33	5	2.179(1)	1.857(3)	85.6(2)	97.44(8)
12	34	5	2.168(11)	1.86(2)	82.9(11)	97.3(4)
			2.146(11)	1.85(3)		
9	28	6,5	2.164(1)	1.940(4)	82.5(2)	95.4(1)

trans species	ref	N,S ring size	Ni−S	Ni−N	N−Ni−N	S−Ni−S
14, X = H, Y = CH_3	36	5	2.198(3)	1.974(10)	180	180
14, X = O═, Y = H	37	5	2.186(2)	1.933(5)	180	180
			2.191(2)	1.915(5)		
14, X = CO_2^-, Y = H	38	5	2.209(4)	1.906(9)	178.6(2)	177.0(1)
			2.199(3)	1.928(9)		
15	39	5	2.159(1)	1.868(3)	180	180

In Ni((*R*,*R*)-**1**) and in Ni(**4**), the Ni−S bond distances are equal to within ±0.01 Å and lie within the narrow range [2.146(11)−2.179(1) Å] reported for a variety of tetradentate *cis*-Ni^{II}N$_2$S(thiolate)$_2$ species (Table 3). In contrast, the Ni−N distances in the five-membered chelate rings of Ni((*R*,*R*)-**1**) are significantly shorter than those in the six-membered chelate rings of Ni(**4**), a pattern that is repeated for species **8**−**13** (Table 3). Further, the data in Tables 2 and 3 also serve to extend a "subtle chelate[28]" or clothespin effect to a wider variety of species: with the Ni ion as the pivot of the clip, as the N−Ni−N angle decreases, the S−Ni−S angle increases, while the sum of the two angles remains near 180°.

While reaction of ligand **6**, a mixture of isomers, with Ni(acac)$_2$ could lead to several products, only the stereo-

(28) Smee, J. J.; Miller, M. L.; Grapperhaus, C. A.; Reibenspies, J. H.; Darensbourg, M. Y. *Inorg.Chem.* **2001**, *40*, 3601−3605.

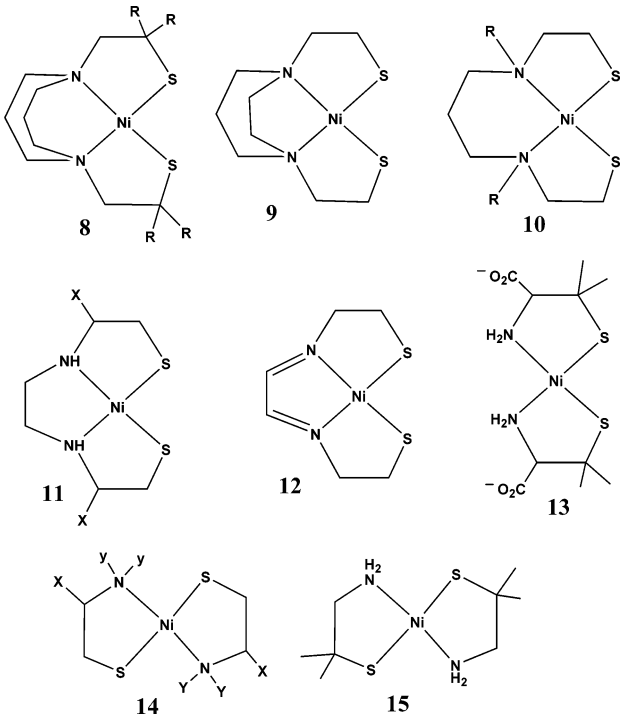

chemically pure dinuclear product (1*S**,3*R**,1′*S**,3′*R**)-**7** was obtained. Mononuclear metal complexes of **6** presumably are precluded by unfavorable eight-membered N,N-chelate rings; further, for the 1*S**,3*R** isomer, molecular models suggest that the distance between N atoms is too large to chelate a Ni(II) ion.

In (1*S**,3*R**,1′*S**,3′*R**)-**7**, **6** behaves as a bis(bidentate) N(amine)S(thiolate) ligand, pairs of which link two Ni(II) centers to form a 16-membered macrocycle (Figure 3). In space group $P\bar{1}$ with $Z = 1$, the dimeric units are necessarily centrosymmetric. Some cyclohexyl and methylene H atoms point toward the centers of the dimers and are in van der Waals contact, precluding the possibility of incorporating a small molecule in the molecular interior. The *trans*-N_2S_2 unit is distorted substantially from square planar, as evidenced, for example, by the S−Ni−S bond angle of 166.18(7)°, which is substantially smaller than the S−Ni−S angles in the four bis(bidentate), *trans*-NiN_2S_2 species shown in Table 3. Further, the tetrahedral-twist angle of 15.00(18)° (Table 2) is unusually large when compared with those of Ni((*R*,*R*)-**1**), Ni(**4**), and the species listed in Table 3. Both the Ni and S atoms exhibit a number of intramolecular contacts with various H and C atoms, which range from 0.23 to 0.87 Å shorter than the sum of their contact radii. The Ni atom exhibits short contacts with C11 and its H atoms and with an H atom from each of the methyl groups C4 and C7. Similarly, the S atoms show short contacts to the H atoms of C9 and C13. The shortest of these interactions with the Ni ion, Ni···H11A, is 2.63 Å and may be indicative of an agostic interaction. Distortion of the coordination geometry is consistent with these short contacts. Intra- and intermolecular Ni···Ni distances of 6.940(2) and 6.127(2) Å (shortest), respectively, suggest little intermetallic interaction.

The N,S-chelate rings adopt the envelope conformation with the flaps, C2 and C6, pointed away from the center of

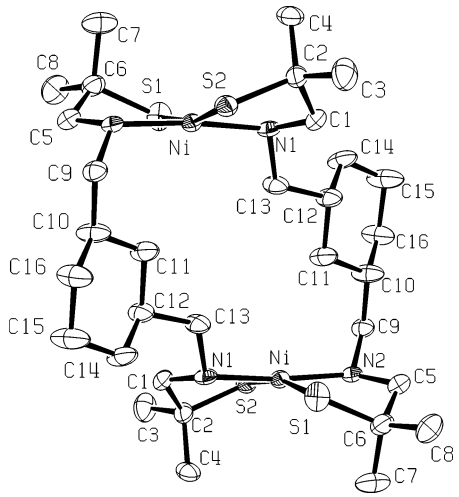

Figure 3. ORTEP[27] view of (1*S**,3*R**,1′*S**,3′*R**)-**7** shown with 30% probability thermal ellipsoids. H atoms have been omitted for clarity.

gravity of the molecule. Both the Ni−S and Ni−N distances are typical for their type (Table 3).

Electronic Spectral Studies. Ni((*R*,*R*)-**1**) (Figure 4 and Table 4) shows ligand-field (LF) bands consisting of a relatively weak low-energy absorption (17 500 cm^{-1}, $\epsilon = 22$) flanked by a more intense absorption at higher energy (21 800 cm^{-1}, $\epsilon = 210$). Similar patterns for LF absorptions have been reported for other diamagnetic, nearly planar NiN_2S(thiolate)$_2$ species such as *trans*-bis(*N*,*N*′-dimethyl-*β*-mercaptoethylamino)nickel(II),[36,40] *cis*-bis(D-penicillaminato-*N*,*S*)nickel(II),[35] and *cis*-*N*,*N*′-dimethyl-*N*,*N*′-bis(2-mercaptoethyl)-1,3-propanediamino)nickel(II),[32] all of whose UV absorptions have only been partially analyzed.[9b,11b,12] A more detailed assignment of the higher-energy bands shown by Ni((*R*,*R*)-**1**) is based upon absorption spectra, augmented by CD spectra, molecular orbital (MO) considerations, and earlier assignments of S,N → Cu(II) ligand-to-metal charge transfer (LMCT) spectra shown by stable aminothiolate complexes of the more oxidizing Cu(II) ion.[41] These approximately planar chromophores all have a $d_{x^2-y^2}$ vacancy as the acceptor orbital for LMCT processes.

The Ni−S−C bond angles in Ni((*R*,*R*)-**1**) (Table 2) imply that the orientation of the Ni−S(thiolate) bonds relative to

(29) Darensbourg, M. Y.; Tuntulani, T.; Reibenspies, J. H. *Inorg. Chem.* **1994**, *33*, 611−613.
(30) Buonomo, R. M.; Font, I.; Maguire, M. J.; Reibenspies, J. H.; Tuntulani, T.; Darensbourg, M. Y. *J. Am. Chem. Soc.* **1995**, *117*, 963−973.
(31) Schneider, J.; Hauptmann, R.; Osterloh, F.; Henkel, G. *Acta Crystallogr.* **1999**, *C55*, 328−330.
(32) Colpas, G. J.; Kumar, M.; Day, R. O.; Maroney, M. J. *Inorg. Chem.* **1990**, *29*, 4779−4788.
(33) Krüger, H.-J.; Peng, G.; Holm, R. H. *Inorg. Chem.* **1991**, *30*, 734−742.
(34) Fernando, Q.; Wheatley, P. J. *Inorg. Chem.* **1965**, *4*, 1726−1729.
(35) Baidya, N.; Olmstead, M. M.; Mascharak, P. K. *Inorg. Chem.* **1991**, *30*, 3967−3969.
(36) Girling, R. L.; Amma, E. L. *Inorg. Chem.* **1967**, *6*, 2009−2012.
(37) Ruble, J. R.; Seff, K. *Acta Crystallogr.* **1972**, *B28*, 1272−1278.
(38) Baidya, N.; Ndreu, D.; Olmstead, M. M.; Mascharak, P. K. *Inorg. Chem.* **1991**, *30*, 2448−2451.
(39) Suades, J.; Solans, X.; Font-Altaba, M. *Polyhedron* **1984**, *3*, 1227−1231.
(40) Root, C. A.; Busch, D. H. *Inorg. Chem.* **1968**, *7*, 789−795.
(41) Stibrany, R. T.; Fikar, R.; Brader, M.; Potenza, M. N.; Potenza, J. A.; Schugar, H. J. *Inorg. Chem.* **2002**, *41*, 5203−5215.

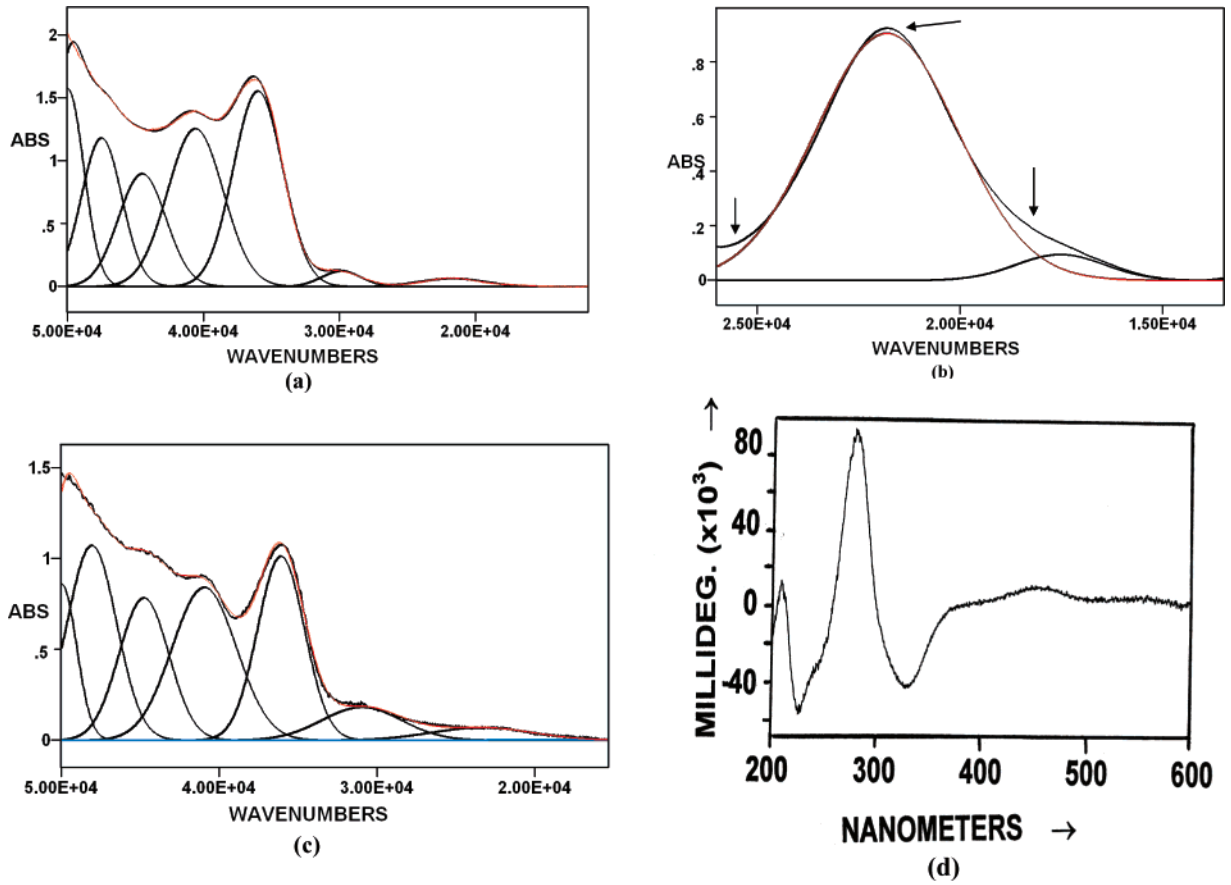

Figure 4. Deconvoluted electronic spectra: (a) Ni((*R*,*R*)-**1**), 1.20 mM solution in water (room temperature, 0.1 cm path length); (b) Ni((*R*,*R*)-**1**), 4.3 mM water solution (room temperature, 1.0 cm path length); arrows indicate the measured spectrum; (c) Ni((*R*,*R*)-**1**), 0.87 mM glycerol/water glass (80 K, path length ≤0.17 cm; see text); (d) Ni((*R*,*R*)-**1**), 1.20 mM in water (room-temperature CD spectrum, path length 0.1 cm).

Table 4. Summary of Deconvoluted Electronic Spectra

system	solution UV−vis energy (cm^{-1})	ϵ per Ni^{II}	solution CD (cm^{-1})	deg × 10^{-3}	80 K glass UV−vis energy (cm^{-1})[a]	assignment	$\Delta\epsilon$	$\lvert\Delta\epsilon\rvert/\epsilon$
Ni((*R*,*R*)-**1**)	17 500	22	18 000	∼+2	∼17 700	LF	0.5	0.023
	21 800	210	22 000	∼+10	23 500	LF	2.5	0.012
	30 000	1000	30 300	-44	30 900	π(S) → Ni(II) LMCT	11	0.011
	36 000	13000	36 000	+90	36 100	σ(S) → Ni(II) LMCT	22.5	0.0017
	40 600	11000	∼40 000	∼-30	41 000	σ(N) → Ni(II) LMCT	7.5	0.00068
	44 500	7500	∼44 000	∼-57	44 600	S	14.3	0.0019
	47 500	10000	47 600	∼+10	44 600	S,N Rydberg	2.5	0.00025
	>50 000				>50 000			
Ni(**4**)	16 600	32				LF		
	21 000	124				LF		
	30 500	<80				LF?		
	33 300	∼3600				π(S) → Ni(II) LMCT		
	36 600	17000				σ(S) → Ni(II) LMCT		
	40 000	13000				σ(N) → Ni(II) LMCT		
	44 700	11000				S		
	48 300	11000				S,N Rydberg		
	>50 000							
(1*S**,3*R**,1′*S**,3″*R**)-**7**	15 200				14 900[b]	LF		
	19 700				20 700[b]	LF		
					27 200[b]	π(S) → Ni(II) LMCT		
					30 600[b]	σ(S) → Ni(II) LMCT		
					36 400[b]	σ(S) → Ni(II) LMCT		
					40 800[b]	σ(N) → Ni(II) LMCT		
					43 700[b]	S		
					45 500[b]	S,N Rydberg		

[a] Owing to light leaks from cracks in the frozen glass, band intensities are not reported. [b] Mineral oil mull, room temperature.

the Ni(II) $d_{x^2-y^2}$ vacancy is consistent with the conventional metal−thiolate bonding view in which M(II)−S bonding consists of one σ-bonding and two nondegenerate π-bonding interactions (Figure 5). In the free thiolate ion, one of the three S lone pairs exhibits considerable S−C bonding character and is more stable than the other two by about 2

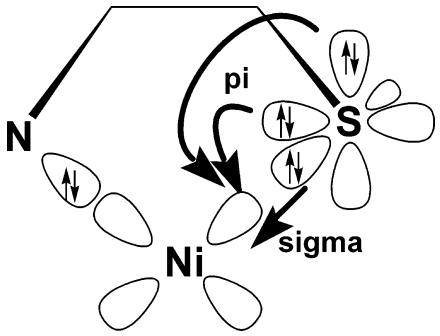

Figure 5. Sketch of a $Ni^{II}N(amine)S(thiolate)$ chromophore showing the interaction of the sulfur and nitrogen valence-shell orbitals with the Ni^{II} d vacancy.

eV.[42a,43] This view of thiolate ligands predicts strong σ(S) → Ni(II) LMCT absorption flanked at lower energy by weaker π(S) → Ni(II) LMCT absorption. The relatively high binding energy and reduced spatial extension of the remaining electron pair, which has substantial S−C bonding character, is expected to result in π(S−C) → Ni(II) LMCT, which is relatively weak and shifted by as much as 16 000 cm^{-1} toward higher energy. Further, this latter band should be obscured by intense σ(N) → Ni(II) LMCT, by localized thiolate absorption, and by ligand Rydberg transitions located in the higher-energy UV spectral region.

The view described above must be modified for the interacting pairs of thiolate orbitals in *cis*- and *trans*-NiN_2S_2 chromophores in which the ligand-based highest occupied MO (HOMO) is the weakly bonding out-of-phase combination of the highest-energy π-symmetry orbital on each thiolate with Ni(II).[9b,11b,12] Consequently, the lowest-energy LMCT absorption of both *cis*- and *trans*-NiN_2S_2 chromophores is π(S) → Ni(II), corresponding to excitation from the ligand-based HOMO into the Ni(II) d vacancy. Owing to the poor overlap and weakness of π bonding relative to σ bonding, π(S) → Ni(II) LMCT bands must be substantially weaker than σ(S) → Ni(II) LMCT bands, and for this reason, a second π(S) → Ni(II) LMCT transition originating from the in-phase combination of the highest-energy π-symmetry thiolate orbital with Ni(II) may be obscured by the more intense σ(S) → Ni(II) LMCT bands, as well as by other absorptions at higher energies. Thus, only one π(S) → Ni(II) LMCT absorption may be observable with conventional electronic or CD spectroscopy.

A similar situation is obtained for the σ-symmetry orbital on each thiolate, except that σ-bonding interactions enjoy better overlaps and σ(S) → Ni(II) LMCT typically shows substantial intensity. MO calculations suggest that differences exist between planar *cis*- and *trans*-NiN_2S_2 chromophores with respect to the thiolate orbital combinations used for σ bonding.[9b] Owing to the more pronounced thiolate electronic coupling across the Ni(II) ion for *trans*-NiN_2S_2 complexes, the bonding and antibonding combinations of the thiolate σ-symmetry orbitals in the ground electronic state were estimated to be split by ∼10 300 cm^{-1}, whereas those for a *cis*-NiN_2S_2 complex only were split by ∼770 cm^{-1}.[9b] Consequently, planar *cis*-NiN_2S_2 chromophores may only show a single nonresolvable σ(S) → Ni(II) LMCT absorption. However, an *approximately trans*-NiN_2S_2 complex may show two such absorptions when structural distortions remove the center of symmetry.

CD measurements can help differentiate between σ(L) → M(II) and π(L) → M(II) LMCT. LMCT absorption from strongly overlapping metal−ligand σ interactions involves linear charge displacement and carries substantial electric dipole allowedness. In contrast, weaker orbital overlap from metal−ligand π interactions has less electric dipole allowedness but requires linear plus rotary charge displacement (Figure 5), giving rise to a greater CD allowedness and a relatively large $\Delta\epsilon$. Thus, the larger $\Delta\epsilon$ and smaller ϵ of the π(L) → Ni(II) LMCT is expected to result in a larger Kuhn factor ($\Delta\epsilon/\epsilon$) than those of the higher-energy σ(S,N) → Ni(II) LMCT absorptions.[42b]

The deconvoluted solution spectrum (Figure 4a) and the better-resolved low-temperature spectrum (Figure 4c) of Ni((*R*,*R*)-**1**) yield comparable results (Table 4). Bands at 30 000 and 36 000 cm^{-1} show energies, separations, and intensities appropriate for π(S) → Ni(II) and σ(S) → Ni(II) LMCT, respectively, an interpretation that is supported by the solution CD spectrum (Figure 4d). The lower-energy LMCT band has a higher (∼6×) Kuhn factor (Table 4) than that of the flanking, more intense LMCT absorption at 36 000 cm^{-1}. An analogous assignment may be made for the absorptions of comparable energies and intensities reported for the bis(D-penicillaminato-*N*,*S*)nickel(II) chromophore.[35] Similar patterns of π,σ(S) → Cu(II) LMCT are shown by *cis*-$CuN_2S(thiolate)_2$ chromophores;[41] however, these absorptions are shifted by ∼6000 cm^{-1} toward lower energies, consistent with the more oxidizing nature of Cu(II) compared with Ni(II).[44]

Both σ(N) → Ni(II) LMCT and thiolate transitions are leading candidates for assigning the intense, higher-energy bands at 40 600 and 44 500 cm^{-1}. These absorptions are expected to be broad because of the relatively large changes in bond strengths associated with such processes. Planar, diamagnetic $Ni^{II}N_4$ chromophores exhibit a broad, intense (ϵ = 11 000−15 000) σ(N) → Ni(II) LMCT absorption in the 40 000−44 600 cm^{-1} range.[45−47] Corresponding σ(N) → Cu(II) LMCT bands shown by $Cu^{II}N_4$ analogues, perturbed somewhat by weak apical axial ligation to oxygen-donor ligands, are red-shifted by ∼6000 cm^{-1}. These σ(N) → Ni(II)/Cu(II) LMCT assignments are supported by the small Kuhn factors of 0.001 and 0.000 56, respectively, shown by chiral $Cu^{II}N_4$ and $Ni^{II}N_4$ complexes.[46] The higher-energy band of Ni((*R*,*R*)-**1**) at 44 500 cm^{-1} is assigned as a localized

(42) (a) Solomon, E. I.; Baldwin, M. J.; Lowery, M. D. *Chem. Rev.* **1992**, *92*, 521−542. (b) Solomon, E. I.; Hare, J. W.; Dooley, D. M.; Dawson, J. H.; Stephens, P. J.; Gray, H. B. *J. Am. Chem. Soc.* **1980**, *102*, 168−178.
(43) Shadle, S. E.; Penner-Hahn, J. E.; Schugar, H. J.; Hedman, B.; Hodgson, K. O.; Solomon, E. I. *J. Am. Chem. Soc.* **1993**, *115*, 767−776.
(44) Knapp, S.; Keenan, T. P.; Zhang, X.; Fikar, R.; Potenza, J. A.; Schugar, H. J. *J. Am. Chem. Soc.* **1990**, *112*, 3452−3464.
(45) Curtis, N. F. *J. Chem. Soc.* **1964**, 2644−2650.
(46) Bryan, P. S.; Dabrowiak, J. C. *Inorg. Chem.* **1975**, *14*, 299−302.
(47) Olson, D. C.; Vasilevskis, J. *Inorg. Chem.* **1969**, *8*, 1611−1621.

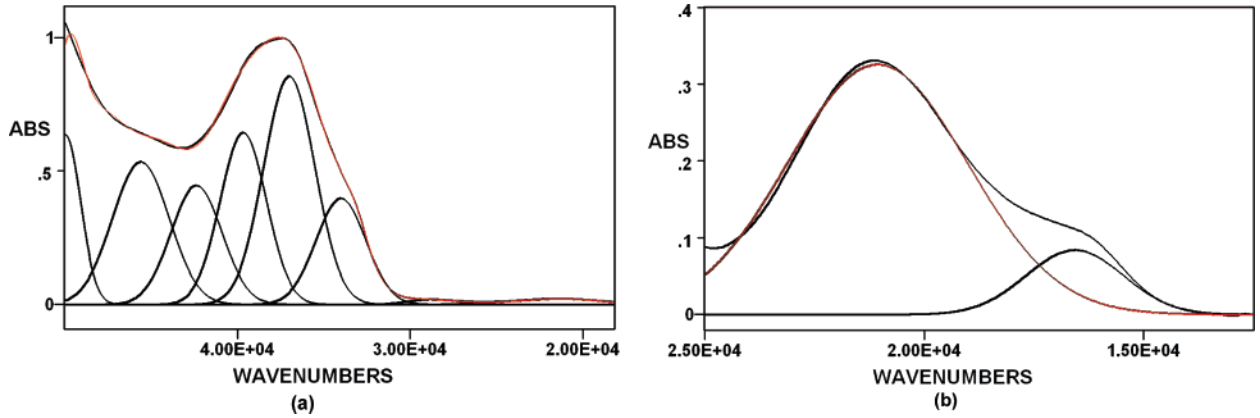

Figure 6. (a) Ni(**4**), 2.49 mM solution in acetonitrile (room temperature, path length 0.02 cm); (b) Ni(**4**), 2.62 mM solution in acetonitrile (room temperature, 1.0 cm path length).

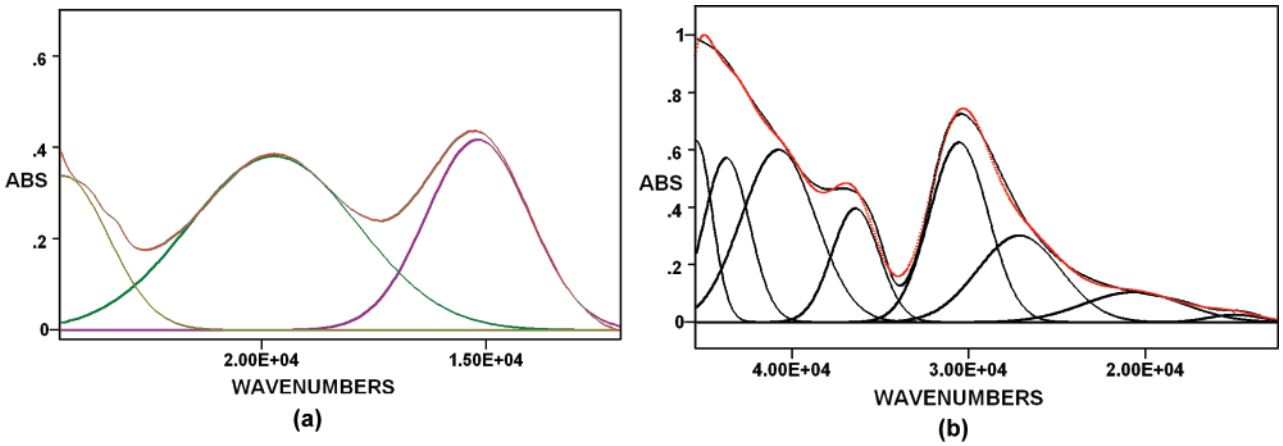

Figure 7. (a) (1*S**,3*R**,1′*S**,3′*R**)-**7**, <2.86 mM solution in methylene chloride with precipitated crystals (room temperature, path length 0.1 cm); (b) (1*S**,3*R**,1′*S**,3′*R**)-**7**, mineral oil mull (room temperature).

thiolate absorption. Both free cysteine and penicillamine, models for the thiolate subunits of Ni((*R*,*R*)-**1**), show strong absorptions in the 43 700−44 700 cm^{-1} region.[48,49] Bands shown by Ni((*R*,*R*)-**1**) at 47 500 and >50 000 cm^{-1} have energies appropriate for thiolate 3p → 4s and amine lone pair → 3s,3p Rydberg absorptions.[50]

Deconvolution of the Ni(**4**) spectra **(**Figure 6a,b) reveals that the positions and intensities of the individual bands in Ni(**4**) are similar to those of Ni((*R*,*R*)-**1**), suggesting comparable band assignments for both complexes. One difference is the weak absorption at 30 500 cm^{-1} shown only by Ni(**4**). A second difference is the separation of 3300 cm^{-1} between the π(S) and σ(S) → Ni(II) LMCT bands at 33 300 and 36 600 cm^{-1}. The corresponding absorptions of Ni((*R*,*R*)-**1**) at 30 000 and 36 000 cm^{-1} show a larger separation of 6000 cm^{-1}. Related *cis*-Cu^{II}N$_2$S(thiolate)$_2$ chromophores with primary and tertiary thiolates show separations of 3700−4000 cm^{-1} between their π(S) and σ(S) → Cu(II) LMCT absorptions.[41]

Extinction coefficients for (1*S**,3*R**,1′*S**,3′*R**)-**7** (Table 4) are not reported owing to its poor solubility in typical organic solvents at room temperature. The complex does dissolve in hot (*T* > 120 °C) DMF, but the strong absorption of DMF in the UV region obscures much of the LMCT bands. For these reasons, spectral analysis was based on the mull spectrum, whose deconvolution affords only qualitative peak heights, owing to light leaks.

Reaction of Ni(II) with H$_2$**6** resulted immediately in surprisingly intense-blue solutions, from which the complex (1*S**,3*R**,1′*S**,3′*R**)-**7** rapidly crystallized. Intense-blue colors normally are shown by approximately tetrahedral Ni(II) chromophores whose LF absorptions have acquired increased intensities by p−d mixing. The two LF absorptions of Ni(1*S**,3*R**,1′*S**,3′*R**-**7**) (Figure 7) differ substantially from those of Ni((*R*,*R*)-**1)** and Ni(**4**): both are abnormally intense with ϵ's > 130. Determination of precise extinction coefficients was precluded by the rapid crystallization of the complex. Judging from the strong initial blue color of the reaction mixture, the true extinction coefficients are probably 2 to 3 times larger. Moreover, the usual intensity relationships of these LF transitions are reversed, with the lower energy more intense than the higher one rather than a factor of 5−10 weaker.

(48) Splittgerber, A. G.; Chinander, L. L. *J. Chem. Educ.* **1988**, *65*, 167−170.
(49) Han, S. M.; Atkinson, W. M.; Purdie, N. *Anal. Chem.* **1984**, *56*, 2827−2830.
(50) (a) Robin, M. B. *Higher Excited States of Polyatomic Molecules*; Academic Press: New York, 1974; Vol. 1, pp 208−219. (b) Robin, M. B. *Higher Excited States of Polyatomic Molecules*; Academic Press: New York, 1974; Vol. 1, pp 276−286.

The *trans*-$Ni^{II}N_2S_2$ chromophore in Ni((1*S**,3*R**,1′*S**,3′*R**)-**7**) differs from those in Ni((*R*,*R*)-**1**) and Ni(**4**) in that it exhibits substantial tetrahedral distortion. Thus, a possible source of the anomalous LF band intensities is more pronounced relaxation of the Laporte restriction due to the loss of a center of symmetry in the Ni((1*S**,3*R**,1′*S**,3′*R**)-**7**) chromophore, which reduces the symmetry from D_{2h} to D_{2d}. This effect was proposed for the anomalously strong ($\epsilon \sim 300$) LF absorptions shown by D_{2d}-distorted tetrachlorocuprate(II) complexes compared to their planar analogues.[51] Intensity stealing via vibronic coupling[52] was considered to be less important owing to the relative weakness of the lowest-energy absorptions shown by tetrachlorocuprates.[53] However, the intensities of S → Ni(II) LMCT bands are greater than those typical of Cl^- → Cu(II) LMCT.[53] Moreover, the mull spectrum of (1*S**,3*R**,1′*S**,3′*R**)-**7** reveals relatively low-energy π(S) and σ(S) → Ni(II) LMCT absorptions at ~27 200 and 30 600 cm^{-1}, respectively. These absorptions are red-shifted by ~6000 cm^{-1} relative to those of Ni(**4**) and Ni((*R*,*R*)-**1**). Comparable red shifts (3000−4000 cm^{-1}) have been reported for the solution spectra of other NiN_2S_2 systems compared to their solid-state reflectance spectra.[40] One interpretation of this result is that LMCT excitation affords Ni(I) and one neutral S, an excited state having reduced charge separation relative to the ground state. Solvents with dielectric constants higher than those experienced by these complexes in their crystal lattices should preferentially stabilize the $Ni^{II}N_2S_2$ ground states.

The tetrahedral distortion in (1*S**,3*R**,1′*S**,3′*R**)-**7** is thought to promote allowedness of a second σ(S) → Ni(II) LMCT at 36 400 cm^{-1}, which originates from the in-phase combination of the thiolate σ-symmetry lone pairs. The higher-energy, localized thiolate absorption at 43 700 cm^{-1}, the σ(N) → Ni(II) LMCT at 40 800 cm^{-1}, and S,N Rydberg absorptions are thought to occur at energies similar to those suggested for Ni((*R*,*R*)-**1**) and Ni(**4**).

Magnetic Susceptibility Studies. The intense-blue color of (1*S**,3*R**,1′*S**,3′*R**)-**7** prompted a magnetic susceptibility study to determine the extent to which the N_2S_2 ligand had imposed tetrahedral coordination on the Ni(II) ion. A finely powdered polycrystalline sample showed a corrected magnetic moment of 0.76 μ_B at 300 K, which slowly decreased to 0.13 μ_B at 5 K, suggesting that this approximately planar d^8 complex shows a modest level of orbital angular momentum, which diminishes with decreasing temperature. Such behavior is possible for the ^3F ground state term whose orbital angular momentum is not fully quenched by the LF.[55] There are some examples of planar Ni(II) complexes whose LFs are insufficiently large to ensure near-diamagnetism.[54] This situation does not apply to (1*S**,3*R**,1′*S**,3′*R**)-**7**.

Summary

Dianion (*R*,*R*)-**1** and molecule **4** act as tetradentate S−N−N−S ligands to form nearly planar *cis*-NiN_2S_2 complexes in which the N−Ni−N and S−Ni−S angles are very nearly supplementary. This "subtle chelate" or clothespin effect has been observed previously[28] and extends to a variety of mononuclear $Ni^{II}N_2S_2$ complexes. Dianion **6** behaves as a bis(bidentate) ligand to form a centrosymmetric, binuclear, *trans*-NiN_2S_2 complex (1*S**,3*R**,1′*S**,3′*R**)-**7**. In contrast to a variety of *cis*- and *trans*-NiN_2S_2 complexes, the coordination geometry in (1*S**,3*R**,1′*S**,3′*R**)-**7** is distorted substantially toward tetrahedral, consistent with a number of short intramolecular contacts involving the Ni and S atoms in the coordination sphere and certain methyl and methylene groups of the ligands. The complexes studied exhibit rich UV−vis spectra, whose deconvoluted bands are assigned, from low to high energy, as LF, π(S) → Ni(II) LMCT, σ(S) → Ni(II) LMCT, σ(N → Ni(II) LMCT, localized S, and S,N Rydberg transitions. Spectral differences include (a) a possible third LF transition for Ni(**4**), (b) an additional σ(S) → Ni(II) LMCT band for (1*S**,3*R**,1′*S**,3′*R**)-**7**, attributed to the in-phase combination of the thiolate lone pairs of σ symmetry, and (c) the unusually intense LF bands for (1*S**,3*R**,1′*S**,3′*R**)-**7**, which are thought to result from relaxation of the Laporte restriction arising from reduction of symmetry of the *trans*-NiN_2S_2 chromophore. The LF band intensities are consistent with a tetrahedral distortion of the coordination sphere and may account for the unexpectedly intense-blue color of (1*S**,3*R**,1′*S**,3′*R**)-**7**.

Acknowledgment. We thank Adam T. Fiedler, Peter A. Bryngelson, Michael J. Maroney, and Thomas C. Brunold for communicating results prior to publication.

Supporting Information Available: Tables in CIF format containing crystallographic data for $[H_3N(CH_2)_3NH_3]$Ni((*R*,*R*)-**1**)·$3H_2O$, Ni(**4**)$_{233}$ and Ni(**4**)$_{298}$, and (1*S**,3*R**,1′*S**,3′*R**)-**7**·2DMF. This material is available free of charge via the Internet at http://pubs.acs.org.

IC050114H

(51) McDonald, R. G.; Riley, M. J.; Hitchman, M. A. *Inorg. Chem.* **1988**, *27*, 894−900.
(52) Larsson, S.; Broo, A.; Sjölin, L. *J. Phys. Chem.*. **1995**, *99*, 4860−4865.
(53) Desjardins, S. R.; Penfield, K. W.; Cohen, S. L.; Musselman, R. L.; Solomon, E. I. *J. Am. Chem. Soc.* **1983**, *105*, 4590−4603.
(54) Frömmel, T.; Peters, W.; Wunderlich, H.; Kuchen, W. *Angew. Chem., Int. Ed. Engl.* **1992**, *31*, 612−613.
(55) *Ligand Field Theory and Its Applications*; Figgis, B. N., Hitchman, M. A., Eds.; Wiley-VCH: New York, 2000; pp 241−268.